Electronic band alignment at CuGaS$_2$ chalcopyrite interfaces

J.E. Castellanos Águila [a,d], P. Palacios [a,b,*], J.C. Conesa [e], J. Arriaga [d], P. Wahnón [a,c]

[a] Instituto de Energía Solar, ETSI Telecomunicación, Universidad Politécnica de Madrid, 28040 Madrid, Spain
[b] Dpt. Física Aplicada a las Ingenierías Aeronáutica y Naval, ETSI Aeronáutica y del Espacio, Pz. Cardenal Cisneros, 3, 28040 Madrid, Spain
[c] Dpt. Tecnología Fotónica y Bioingeniería, ETSI Telecomunicacin, Ciudad Universitaria, s/n, 28040 Madrid, Spain
[d] Instituto de Física, Benemérita Universidad Autónoma de Puebla, Av. San Claudio y 18 Sur, C.U. 72570 Puebla, Mexico
[e] Instituto de Catálisis y Petroleoquímica, CSIC, Marie Curie 2, Cantoblanco, 28049 Madrid, Spain

ABSTRACT

Cu-chalcopyrite semiconductors are commonly used as light absorbing materials on solar cell devices. The study of the heterointerfaces between the absorbent and the contact materials is crucial to understand their operation. In this study, band alignments of the heterojunctions between CuGaS$_2$ chalcopyrite and different semiconductors have been theoretically obtained using density functional theory and more advanced techniques. Band alignments have been determined using the average electrostatic potential as reference level. We have found that the strain in the heterointerfaces plays an important role in the electronic properties of the semiconductors employed here. In this work CuAlSe$_2$/CuGaS$_2$ and CuGaS$_2$/ZnSe heterointerfaces show band alignments where holes and electrons are selectively transferred through the respective heterojunctions to the external contacts. This condition is necessary for their application on photovoltaic devices.

1. Introduction

Solar cells based on chalcopyrite semiconductors of the form Cu(In, Ga)(S, Se)$_2$ have demonstrated high energy conversion efficiencies and their manufacturing is being and important technology in thin film photovoltaics [1,2]. Bang-gap value in these chalcopyrite materials goes from 1.0 eV for CuInSe$_2$ [2] to 2.4–2.53 eV for CuGaS$_2$ [3]. This allow to tune the optoelectronic properties using alloys.

Thin film solar cell structure includes layers of different materials. The formation of interfaces between them plays an important role in the optimal performance of the solar cell device. Although the efficiencies found for these chalcopyrite solar cells at laboratory level are close to the maximum theoretical value [4], much lower efficiencies are obtained using the large scale manufacturing fabrication methods. Furthermore, recent studies have shown that the selection of the buffer layer material plays a very important role in the optimal performance of a solar cell device [5].

The changes observed in the performance of solar cells as a function of the layers chosen as current extracting contacts, which will affect the electronic parameters of the heterojunctions, have hindered a systematic approach to the design of optoelectronic devices. In particular it has been reported that one of the properties that characterizes the interface between two semiconductors is the band offsets [6,7]. The importance of knowing the relative alignment of the valence and conduction bands, lies in the confinement of electrons and holes in the heterostructure, i.e., if we have a type I offsets, electrons and holes are confined at the same side of the heterostructure, whereas if we have a type II offset, electrons and holes are confined at different sides of the heterojunction [8].

To determine the band alignment between two semiconductors, we use a periodic solid model [9]. This method arises from the need to associate the energy levels of the semiconductors which comprise the heterostructure with a common reference energy level which will be an average electrostatic potential. The importance of this model lies in the possibility to determine, using first principle calculations, the band alignment shifting due to strain and orientation [10]. However, this model has the same problem as any ab initio DFT calculation which is to subestimate the band-gap. Therefore, a correct reproduction of the bulk band-gap must be necessary for achieving a successful theoretical description. To solve this problem, the use of hybrid functionals in DFT calculations, has been increasingly applied to study a large variety of periodic systems. The aim of this paper is to present accurate theoretical results (using hybrid functionals) of the band alignment between the conduction and valence band edges of CuGaS$_2$ (a light absorber which has interest as possible component of inexpensive

chalcopyrite-based tandem cells) and those of semiconductor candidates that can be used as contacts for it in solar cells, in particular, CuAlSe$_2$, CdS, ZnSe and ZnS. The results obtained here, may also provide the fundamentals for the design and development of solar cells with an intermediate band [11], based on CuGaS$_2$, which has been proposed as a suitable host semiconductor material developing such band when a transition metal is added to substitute the Gallium atoms [12–16].

2. Model and computational technique

In this paper we have made ab initio DFT theoretical calculations of the structural and electronic properties for different chalcopyrite-semiconductor interfaces. All the calculations were performed using the Vienna ab initio simulation package (VASP) [17]. The core–valence interaction was described by the frozen-core projector augmented wave (PAW) method [18]. The energy cutoff for the plane-wave expansion was set to 350 eV. The Brillouin zone sampling was performed with the Monkhorst–Pack special k-point-mesh [19]. For the slab model used here, and explained below, a $6 \times 2 \times 1$ mesh was used ($6 \times 2 \times 2$ in the bulk calculations). For standard DFT calculations, the exchange–correlation energy has been treated within the generalized gradient approximation (GGA) approximation using the Perdew, Burke, and Ernzerhoff parametrization [20]. It is well known that conventional GGA calculations fail to predict the magnitude of the energy band-gaps. However, it has been shown that the screened hybrid Heyd–Scuseria–Ernzerhof functional (HSE06) [21] presents a significant improvement over the GGA for computing the structural and electrical properties (lattice constant, and band-gaps) of bulk II–VI compound semiconductors [22]. HSE06 functional includes a fraction, α, of short-range Hartree–Fock (HF) exchange to improve the derivative discontinuity of the Kohn–Sham potential occurring for an integer number of electron, as well as a length scale defined by a parameter, ω, where the short-range HF exchange is computed.

The (α, ω) space has been explored only sparsely with results suggesting that different choices of α and ω may improve in a similar way the accuracy of different physical properties. Since the percentage of HF exchange and length scale in a hybrid functional are not universal constants, and the optimal values may be system-dependent, it is worthwhile to study the variation of the band-gaps as a function of α and ω in the HSE06 approximation. Fig. 1 shows the effect of the α and ω parameters on the band-gap for the semiconductors studied in this work. We can observe that a large α value (which is equivalent to a smaller screening of the exchange

interaction) increases the band-gap, while the band-gap decreases for large values of ω, as increasing this latter parameter decreases the spatial range in which the exchange interaction is applied. Fig. 1a shows a linear correlation between α and the band-gap; meanwhile Fig. 1b shows a non-linear dependence when ω increases. The curves displayed in Fig.1, were obtained by a fit procedure of the obtained results by minimizing the least-square error in the band-gaps. The experimental band-gap values can be reproduced accurately by fitting any (or both) of the two parameters. It has been demonstrated that the mixing parameter α can be made equal to the inverse of the dielectric constant of semiconductors, and adjusted consequently to obtain an accurate value of its band-gap [23]. Based on the above, the parameter ω in HSE06 is fixed at the standard value of 0.20 Å^{-1} while α is fitted for each material to reproduce its band gap.

The fraction of HF mixing α, is modified to 0.347, to obtain a band-gap of CuGaS$_2$ (2.43 eV), which agrees with experiment (2.4–2.53 eV) [3]. For CuAlSe$_2$, CdS, ZnSe and ZnS, the α parameter also is modified (0.352 for CuAlSe$_2$, 0.354 for CdS, 0.369 for ZnSe, and 0.306 for ZnS) to reproduce as closely as possible their experimental band-gaps (2.49 eV for CuAlSe$_2$ [24], 2.37 eV for CdS [25], 2.82 eV for ZnSe [25] and 3.52 eV for ZnS [25]). In summary, for each pure semiconductor we determine the α value that allows reproducing exactly the experimental band-gap; with the cell dimensions and atomic parameters obtained through relaxations at the GGA level. This value is significantly higher than the standard one in the HSE06 functional ($\alpha = 0.25$). To calculate the alignment of the band energies between two semiconductors, we construct a supercell that includes one slab for each material and has one interface between them at the center of the supercell. We considered four specific interfaces, CuGaS$_2$/CuAlSe$_2$, CuGaS$_2$/CdS, CuGaS$_2$/ZnSe and CuGaS$_2$/ZnS. The surface of contact, (1 0 2) for CuGaS$_2$ and CuAlSe$_2$, and (1 1 0) for CdS, ZnSe and ZnS, was chosen to be a non-polar termination and able to form cation–anion bonds across the interface, minimizing any charge accumulation. The constructed slab contains eight atomic layers for both materials in each slab. For an adequate match between two non polar surfaces, the 2D surface lattice dimensions must be made equal. The (1 0 2) surfaces of CuGaS$_2$ and CuAlSe$_2$ have 2D rectangular cells of 5.33 Å $\times$ 15.1 Å and 5.66 Å $\times$ 15.89 Å size, respectively; while the (1 1 0) surfaces of CdS, ZnSe and ZnS have approximately 1×2 rectangular 2D cells of 5.88 Å $\times$ 16.63 Å, 5.56 Å $\times$ 15.73 Å and 5.45 Å $\times$ 15.41 Å, respectively. We have different lattice parameters to the left and right side of the interface. We construct the unrelaxed supercell with inter-planar distance equal to the average between the inter-planar distances of the
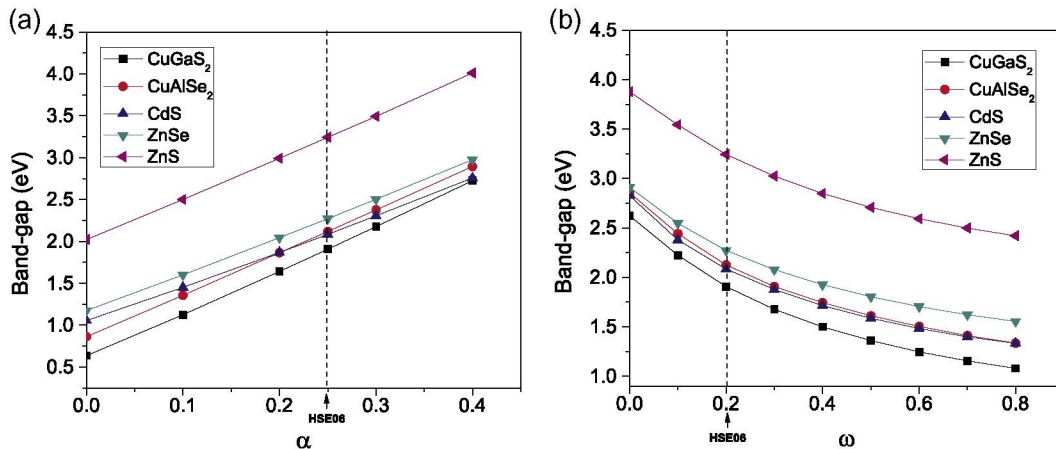

Fig. 1. Calculated band-gap vs (a) fraction of α HF mixing, and (b) the parameter ω (in units of Å^{-1}) which defines the range of the exchange interaction.

constituent semiconductors. The same was done for the lattice constants parallel to the interface. The basic unit cell is periodically repeated in space in order to generate an infinite system. For the non-polar surface chosen $(10\overline{2})$, the minimum number of atomic layers to reproduce the structural and electronical properties of $CuGaS_2$ are eight layers, giving a total of 64 atoms for each slab, and 128 atoms for the heterostructure. Increasing the size of the supercell in a direction parallel to the interface involves duplicating the number of layers. This is too much to be handled with our present resources. We have studied a supercell with 16 layers of $CuGaS_2$ and 8 layers for the semiconductor contact. The changes of the structural properties and the electrostatic potential for the slab model are negligible.

Fig. 2 shows the structure of the supercell used to represent the interface in the direction $(10\overline{2})$. Even though periodic boundary conditions are imposed along the planes parallel to the interface to simulate an infinite system, the heterointerface displays the special constraints of the relatively small size of the slabs used in the simulation. Consequently, it is favorable for the atomic spacing on either side of the interface to slightly contract and expand the lattice parameters of each material to align with adjacent atoms, while the atoms farthest away from the interface optimize their respective lattice parameters in the direction perpendicular to the interface. Since the structures exhibit a smooth transition from the $CuGaS_2$ to semiconductor material, the interfacial strain is minimized and the only strain remaining in either material just a few atomic planes away from the interface is that due to the change in the lattice dimensions parallel to the slabs.

To obtain the valence- and conduction-band discontinuities, we used an electrostatic potential-based alignment method [9,26] following a three-step computational procedure. The first step is the determination of the appropriate α value for each bulk semiconductor, carried out as said above. Next, structural relaxations for the slab models are carried out at GGA–PBE level. The electrostatic potential distribution is then determined for the optimized geometry results. The electrostatic potential calculations for the slab models wer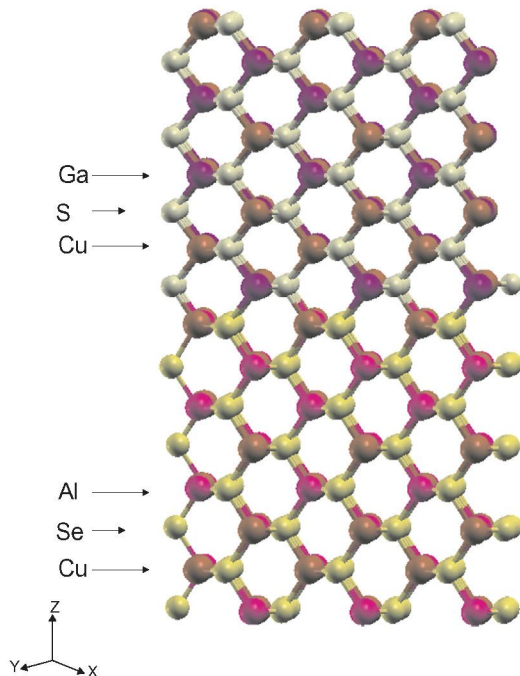e not made with the HSE-α functional, since these calculations are computationally too demanding for large unit cells and the electrostatic potential is already well described using GGA functionals. Besides, it is no clear which α values should be used for such calculation involving two different semiconductors. In the third step it is necessary to perform electronic and electrostatic calculations for the corresponding bulk materials forming the interface. But since these are distorted due to the epitaxial strain, we took the lattice constants and atomic coordinates from the central part of each slab in the model. This is done to calculate the band-gap of the semiconductors under conditions similar to those in the interface model. These calculations were done with the HSE hybrid functional, using the optimum α value obtained before for each relaxed, non-strained pure semiconductor. Then the positions of the band edges relative to the electrostatic potential distribution in each bulk semiconductor were noted, and transferred to the corresponding slab interface model to locate the positions of the band edges for the constituting semiconductors.

3. Results and discussion

Generally thin films develop a large amount of intrinsic stress during the growth of the heterostructures. The presence of stress can not only affect the layer morphology but can also severely modify the electronic properties.

In Table 1, we present the calculated lattice mismatch (only for the x direction) between the $CuGaS_2$ and the different semiconductors involved in the four interfaces proposed. The lattice mismatch is defined as $f = (a - a_{CuGaS_2})/a_{CuGaS_2}$, where a and $a_{(CuGaS_2)}$ are, the lattice constant in the x direction of the contact material and of $CuGaS_2$, respectively. In all cases we can observe that the theoretical values of the lattice mismatch are larger than the experimental values, this is due to the overestimation of the lattice constant produced by standard GGA calculations. Furthermore, the lattice mismatch determines the magnitude of the structural variation displayed by the different types of heterointerfaces, whose magnitude modifies the electronic properties of the semiconductors when forming the heterostructure [27,28]. This modification will affect the type of band alignment.

Table 2 contains the values of band-gaps obtained for each semiconductor using such HSE modified functional (i.e. with the α value giving for the relaxed bulk semiconductor the exact experimental gap) but with the cell parameters obtained from the relaxed slabs. As mentioned above, the structurally induced variations from the band-gaps are a consequence of the internal stresses produced by compression or stretching of the bonds and by changes in the bond angles. In all cases showed in Table 1, for $CuGaS_2$ the band-gap decreases because the lattice constant increases [29]. This is mostly attributed to the coupling between filled anion p and cation d levels, which is large in these chalcopyrites because the elements of the group IB in the periodic table have high d orbital energies, and the coupling is inversely proportional to the energy separation between the anion p and cation d energy states; this coupling is then rather sensitive to the anion–cation distances and to the symmetry around the atoms. On the other hand, all the semiconductors forming the other side of the four interfaces are under internal compression, which is accompa-

Fig. 2. Structure of the supercell for the $CuGaS_2/CuAlSe_2$ $(10\overline{2})$ interface. Other chalcopyrite heterointerfaces supercells are constructed similarly.

Table 1
Theoretical and experimental lattice mismatch (f) between different semiconductors and $CuGaS_2$ (in % with respect to the $CuGaS_2$ lattice constant).

System	GGA	Exp.
$CuGaS_2/CuAlSe_2$	5.96	4.86
$CuGaS_2/CdS$	10.47	8.74
$CuGaS_2/ZnSe$	6.58	5.94
$CuGaS_2/ZnS$	1.48	1.10

	CuGaS$_2$/CuAlSe$_2$	CuGaS$_2$/CdS	CuGaS$_2$/ZnSe	CuGaS$_2$/ZnS
HSE-α	2.25/2.70	1.88/2.62	2.16/2.87	2.34/3.55

nied by an opening of the band-gap as it can be clearly seen in Table 2, being the CdS case the most significant. This is consistent with the behavior of the ionicity in semiconductors under pressure [30].

The valence band offset for each interface, ΔE_V, is calculated following the scheme said above, as

$$\Delta E_V = \Delta EP_{step} + \Delta E_{VB} - \Delta EP \qquad (1)$$

where ΔEP_{step} is the difference between the two semiconductor reference levels (the two averages of the maximum values of the electrostatic potential in the center of each slab) obtained from the slab calculation. Note that throughout this article the electrostatic potential values are given always multiplied by the electron charge, with its sign, so that they have energy units. ΔE_{VB} (ΔEP) is the difference between the edges of the valence bands (the electrostatic potential-based reference levels) as obtained from two independent bulk calculations of the single phases at the same strained geometries as in the relaxed slab construction. The conduction band offset is determined from ΔE_V and the difference in bulk band-gaps of the corresponding distorted pure semiconductors, ΔE_g, as

$$\Delta E_C = \Delta E_V + \Delta E_g \qquad (2)$$

In Fig. 3a, we present the average of the electrostatic potential (EP) computed in planes parallel to the interface between the two semiconductors, for the CuAlSe$_2$/CuGaS$_2$ slab model. The dotted line in the center denotes the position of the interface. We observe that the electrostatic potential suffers a distortion for planes near to the interface, being the CuGaS$_2$ the strongest affected. The electrostatic potential is non-periodic for layers near to the interface, and goes asymptotically into two different periodic functions for layers far away from the interface. The EP oscillates within each slab near the interface but reaches near the slab center a constant value. The discontinuity in this reference potential across the interface is defined as $\Delta EP_{step} = EP_{CuAlSe_2} - EP_{CuGaS_2} = (4.04 - 3.50)$ eV, being 4.04 and 3.50 eV the electrostatic potential for CuAlSe$_2$ and CuGaS$_2$ respectively. Results for the other cases were also obtained in a similar way. The electrostatic potential obtained for both distorted semiconductors, CuGaS$_2$ and CuAlSe$_2$, can be seen in Fig. 3b), which includes the top of the valence band (E_{VB}), and the lowest of the conduction band (E_{CB}). The difference between (E_{VB}) values is 0.48, whereas the difference between the electrostatic potential for these semiconductors is $\Delta EP = 0.86$ eV.

Fig. 4 shows the variation of the electrostatic potential and the band-gap of CuGaS$_2$ as a function of the lattice mismatch (generated by the different interfaces). In any case, the comparison provides clear evidence that the electrostatic potential and band-gap shifts is due to the effect of tensile stress. According to the solid model theory [10], the average electrostatic potential is inversely proportional to the volume of the unit cell. So it is important to consider changes in the lattice constant for each of the materials forming the heterostructure. Particularly, for the case of CuGaS$_2$, at large lattice mismatch (which in this case implies an increase in lattice constant), the average electrostatic potential tends to decrease, leading to the shifting of the valence and conduction bands at higher energies. The variation of the band-gap as a function of the lattice mismatch, shows the same behavior as the electrostatic potential, the band-gap decreases with an increase in the

lattice constant, and the band gap difference is distributed between the valence band offset (ΔE_V) and the conduction band offset (ΔE_C).

These two effects, an more particularly the presence of strain in the heterostructure, can directly affect the nature of the band alignments at the lattice-matched interfaces passing from the straddling gap (type I) to staggered gap (type II) or vice versa. Our band alignments can be compared directly to the prediction of Anderson's electron affinity rule, which states that the conduction band offset (ΔE_C) would then be given by the difference in electron affinity of the two semiconductors, while the valence band offset (ΔE_V) is given by the difference between the band-gap difference and the conduction band offset [31]. The electron affinity of the CuGaS$_2$ is about 4.1 eV [32], for the CuAlSe$_2$ is 3.8 eV [32], and for the CdS, ZnSe and ZnS are 4.3 eV [33], 4.09 eV [33], and 3.9 eV [34], respectively. The electron affinity rule would predict for the CuGaS$_2$/CuAlSe$_2$, CuGaS$_2$/ZnSe and CuGaS$_2$/ZnS interfaces a band alignment of type I (electron confinement in CuGaS$_2$). These results are consistent with those reported for Chichibu et al. [32]. However, for the CuGaS$_2$/CdS interface, Anderson's rule yields a type II line up, with the valence and conduction-band of CdS below of the valence and conduction-band of the CuGaS$_2$ (0.27 and 0.2 eV, respectively).

However, according to our results, the band alignments differ substantially as the lattice mismatch increases. Table 3 shows the GGA and HSE-α calculated valence and conduction band offsets of the four specific heterointerfaces proposed. We have used a sign convention such that a positive value of the band offset for the discontinuity at the junction A/B corresponds to an upward step in going from A to B as employed in Ref. [9]. It includes also, for comparison, the values that would be found if only GGA, not HSE-α, had been used throughout. Although both GGA and HSE-α give similar band offsets, the former should not be relied upon since GGA underestimates the band-gaps of both constituents; similar offset values will be obtained only when the GGA band-gap error is similar for both semiconductors in the interface. However, HSE-α predicts the nature and magnitude of band-gaps accurately. This is especially relevant in the CdS case which shows the largest band-gap error in our GGA calculations. The importance of considering the distortion and the HSE-α approximation in the band alignments, is reflected in comparison with Anderson's electron affinity rule results.

In this rule the main contribution to the change in the type of alignment is due to a modification in the band-gap caused by the tensile stress generated by the interface.

Fig. 5 shows a schematic representation of the band-alignment at the interfaces between CuGaS$_2$ and all the other semiconductors considered in this work. From the figure, the CuGaS$_2$/CuAlSe$_2$ interface is type II and possesses a staggered alignment, with both the valence and conduction bands of CuGaS$_2$ lying in energy below the corresponding one of CuAlSe$_2$. Within the approximations of our calculations, CuGaS$_2$ and CuAlSe$_2$ topmost valence band are almost aligned, and an offset of 0.16 eV is predicted. The barrier in the conduction bands is mainly due to the difference in the bands-gaps of both materials and equals to 0.62 eV. The CuGaS$_2$/CdS interface is of type I, meaning that the band-gap of CuGaS$_2$ lies completely inside the band-gap of CdS. More specifically, the ΔE_V of CuGaS$_2$ is 0.62 eV higher than that of CdS while its ΔE_C is only 0.12 eV less than that of CdS. This result is consistent with the empirical work of Singh et al. [5], where the CuGaS$_2$/CdS interface exhibits poor conversion efficiency. They suggest that the lattice mismatch is an important factor in the performance of the solar cell device; we show here that in any case the band alignment is inadequate in this system. The CuGaS$_2$/ZnSe heterointerface exhibits a type II (staggered) band lineup. The corresponding band offset for this interface gives ΔE_V and ΔE_C equal to 0.87 eV and
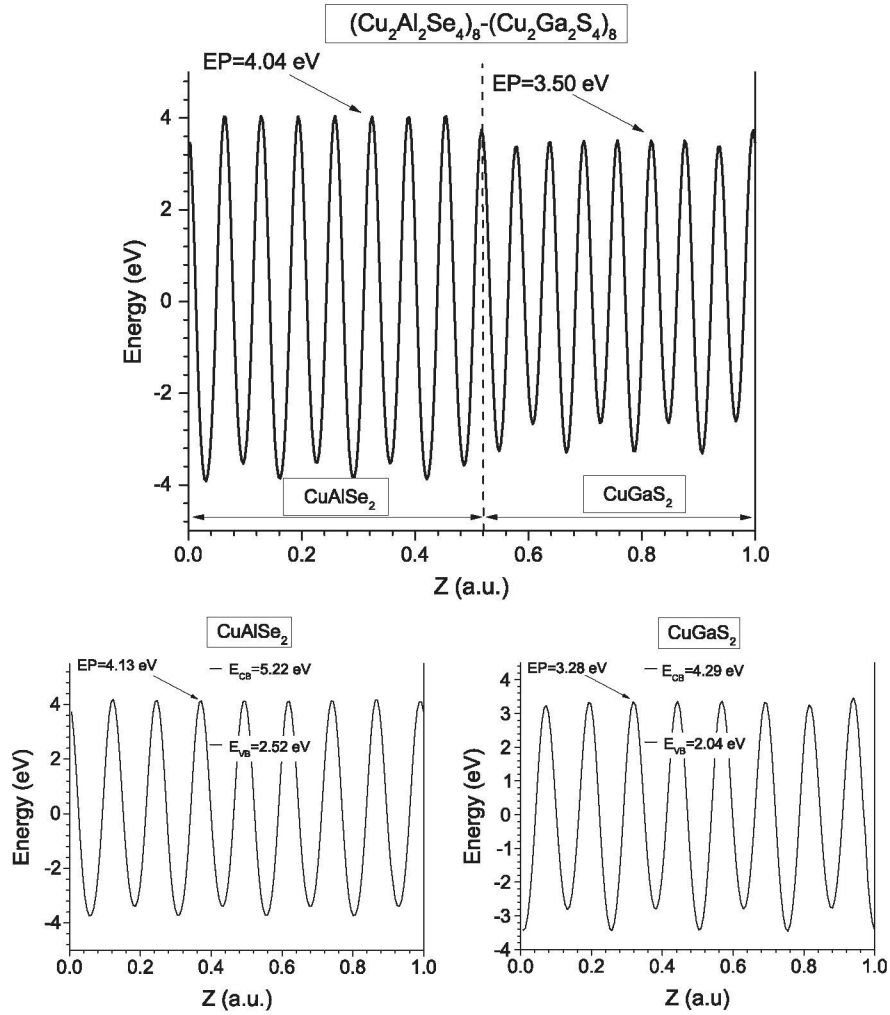
Fig. 3. (a) Planar average of the electrostatic potential of CuGaS$_2$/CuAlSe$_2$ (1 0 2) oriented along this direction. The reference level is determined by this potential at positions intermediate between the atomic planes which are far from the interface. (b) Electrostatic potential and energy levels of the gap edges, obtained for CuAlSe$_2$ and CuGaS$_2$ single phases distorted due to the epitaxial strain.
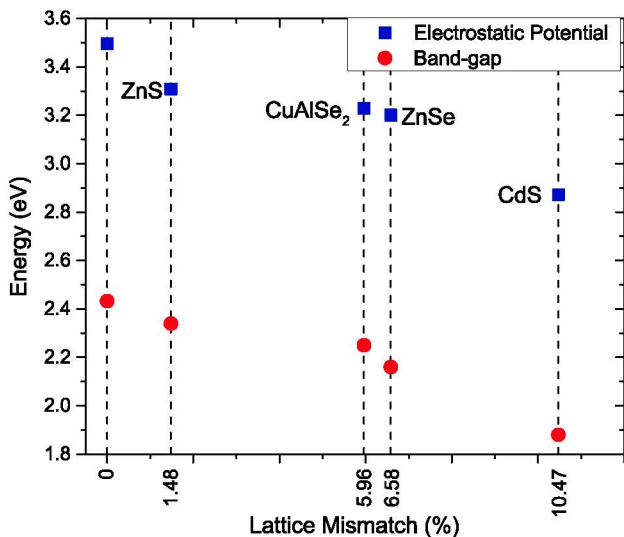
Fig. 4. Electrostatic potential and band-gap variation of CuGaS$_2$ versus the lattice mismatch. The lattice mismatch values are taken from Table 1 and correspond to the four interfaces studied here. The EP and band-gap are obtained from the corresponding four distorted bulk calculations.
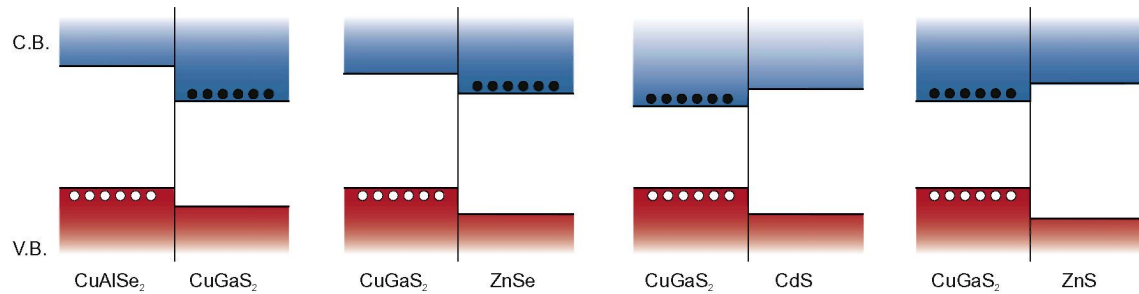
0.15 eV respectively, with CuGaS$_2$ bands lying higher. Finally, the CuGaS$_2$/ZnS interface is of type I. The conduction and the valence bands of the CuGaS$_2$ are inserted within the band-gap of the wide-gap semiconductor (ZnS). A downward step of 0.84 eV for the valence band is theoretically obtained which implies a ΔE_C of 0.38 eV. In this case, the large band-gap differences are the main factor in the type of alignment. So the electrons and holes are thermalized on the same side of the interface.

As stated in Table 3 and considering the difference between type I and type II heterojunctions, the band offsets have different signs at the type I interface. For this type of band alignment, occurring here at the interfaces with CdS and ZnS, electrons and holes are localized on the same side of the interface, i.e. in the narrow-gap layer which in this cases is CuGaS$_2$. This leads to an easy recombination of the carriers inside CuGaS$_2$, from which they cannot escape. At the type II interface, where the band offsets have the same sign, electrons and holes localize on different sides of the interface, facilitating thus only recombination through spatially indirect transitions.

According to the results obtained in this work, in a photovoltaic device using as light absorber CuGaS$_2$, CuAlSe$_2$ can be used to achieve selective hole collection, while ZnSe can be used for selective electron collection. For CuGaS$_2$/CdS interface, for which the Anderson's rule predicts a staggered gap, meaning that the valence

Table 3
Calculated valence (ΔE_V) and conduction (ΔE_C) band offsets (in eV) for different hererointerfaces referred to the valence band of $CuGaS_2$.

	$CuGaS_2/CuAlSe_2$		$CuGaS_2/CdS$		$CuGaS_2/ZnSe$		$CuGaS_2/ZnS$	
	GGA	HSE-α	GGA	HSE-α	GGA	HSE-α	GGA	HSE-α
ΔE_V	0.21	0.16	−0.45	−0.62	−0.71	−0.87	−1.05	−0.84
ΔE_C	0.69	0.62	−0.40	0.12	−0.08	−0.15	0.42	0.38

Fig. 5. Band alignments between the $CuGaS_2$ and several wide band gap semiconductors proposed as contacts, computed with HSE-α.

and conduction bands in CdS are lower in energy than the valence and conduction-bands in $CuGaS_2$, our result shows on the contrary, as said above, a straddling gap, which is an incorrect band alignment for photovoltaic applications, but is often used to fabricate light emitting diodes and lasers [35,36]. This example shows how the effects of the lattice mismatch can modify the valence and conduction-bands discontinuities at which the $CuGaS_2/CdS$ interface switches from type II to type I. Finally, the structural and electronic results suggest that the nanostructure $CuAlSe_2/CuGaS_2/ZnSe$ may improve the carrier collection efficiency, which would allow to build a p–i–n heterostructure. Tandem solar cells can thus be made using this structure for the front (high band gap) side of the cell. Alternatively, if suitable transition metals are used to substitute for Gallium atom in the $CuGaS_2$ chalcopyrite, an intermediate band solar cell could be made, which could potentially improve the performance of a solar cell [16]. The appropriate level of cationic substitution to form and intermediate band using transition metal atoms is about a 10%. At this level of metal concentration the main gap will be affected by less than one or two tenths of eV [37] so the band alignment should not change significantly.

4. Conclusions

In summary, we have presented density functional calculations of the band alignment and structural properties for the $CuAlSe_2/CuGaS_2$, $CuGaS_2/CdS$, $CuGaS_2/ZnSe$ and $CuGaS_2/ZnS$ heterointerfaces. The HSE-α hybrid functional used reproduces accurately experimental band-gaps and hence correct band offsets can be expected using it. We also discuss the effects of the lattice mismatch on the electrostatic potential and on the band-gap, that describe the variation on the type of the band alignments. This effect is relevant for the study of the $CuGaS_2/CdS$ interface where the band alignment changes from type II to type I. The alignment using as reference the average electrostatic potential predicts that the $CuGaS_2/CuAlSe_2$ and the $CuGaS_2/ZnSe$ interface are type II and possess a staggered alignment. The valence and conduction bands of $CuGaS_2$ lie at energies below the corresponding ones of $CuAlSe_2$. For ZnSe just the opposite happens, $CuGaS_2$ valence and conduction bands lie at energies above the corresponding ZnSe bands. These are the appropriate conditions to match two interfaces into a heterostructure with three semiconductors ($CuAlSe_2/CuGaS_2/ZnSe$) so that electrons and holes photo-generated in $CuGaS_2$ (used

as light absorber) can be extracted selectively, as desired, at both device sides. The detailed model employed here, should serve as an accurate tool for the quantitative prediction of band alignment at heterojunctions for which no experimental data yet exist.

References

[1] P. Jackson, D. Hariskos, E. Lotter, S. Paetel, R. Wuerz, R. Menner, W. Wischmann, M. Powalla, Prog. Photovolt.: Res. Appl. 19 (7) (2011) 894–897.
[2] S. Siebentritt, Thin Solid Films 403–404 (0) (2002) 1–8.
[3] B. Tell, J.L. Shay, H.M. Kasper, Phys. Rev. B 4 (1971) 2463–2471.
[4] K. Ramanathan, M.A. Contreras, C.L. Perkins, Sally Asher, F.S. Hasoon, J. Keane, D. Young, M. Romero, W. Metzger, R. Noufi, J. Ward, A. Duda, Prog. Photovolt.: Res. Appl. 11 (4) (2003) 225–230.
[5] P. Singh, R. Gautam, S. Sharma, S. Kumari, A.S. Verma, Sci., Measur. Technol., IET 8 (5) (2014) 294–303.
[6] J. Junquera, M. Zimmer, P. Ordejón, P. Ghosez, Phys. Rev. B 67 (15) (2003) 155327.
[7] M.P.C.M. Krijn, Semicond. Sci. Technol. 6 (1991) 27–31.
[8] P.Y. Yu, M. Cardona, Fundamentals of Semiconductors, third ed., Springer, New York, 1996.
[9] C.G. Van de Walle, R.M. Martin, Phys. Rev. B 34 (1986) 5621–5634.
[10] C.G. Van de Walle, Phys. Rev. B. 39 (1989) 1871–1883.
[11] A. Luque, A. Martí, Phys. Rev. Lett. 78 (1997) 5014–5017.
[12] P. Palacios, K. Sánchez, J.C. Conesa, J.J. Fernández, P. Wahnón, Thin Solid Films 515 (15) (2007) 6280–6284.
[13] P. Palacios, I. Aguilera, P. Wahnón, J.C. Conesa, J. Phys. Chem. C 112 (25) (2008) 9525–9529.
[14] P. Chen, M. Qin, H. Chen, C. Yang, Y. Wang, F. Huang, Phys. Stat. Solidi (a) 210 (6) (2013) 1098–1102.
[15] I. Aguilera, J. Vidal, P. Wahnón, L. Reining, S. Botti, Phys. Rev. B (2011) 085145.
[16] I. Aguilera, P. Palacios, P. Wahnón, Sol. Energy Sol. Cells 94 (11) (2010) 1903–1906.
[17] G. Kresse, J. Hafner, Phys. Rev. B 47 (1993) 558–561.
[18] P.E. Blöchl, Phys. Rev. B 50 (1994) 17953–17979.
[19] H.J. Monkhorst, J.D. Pack, Phys. Rev. B 13 (1976) 5188–5192.
[20] J.P. Perdew, K. Burke, M. Ernzerhof, Phys. Rev. Lett. 77 (1996) 3865–3868.
[21] J. Heyd, G.E. Scuseria, M. Ernzerhof, J. Chem. Phys. 118 (18) (2003) 8207–8215.
[22] F. Gygi, Phys. Rev. Lett. 102 (2009) 166406.

[23] M.A.L. Marques, J. Vidal, M.J.T. Oliveira, L. Reining, S. Botti, Phys. Rev. B 83 (2011) 035119.

[24] Y. Shim, K. Hasegawa, K. Wakita, N. Mamedov, Thin Solid Films 517 (4) (2008) 1442–1444.

[25] K.K. Ng, S.M. Sze, Physics of Semiconductor Devices, third ed., WILEY-VCH Verlag, Berlin GmbH, 2007.

[26] J.C. Conesa, J. Phys. Chem. C 116 (35) (2012) 18884–18890.

[27] H. Asai, K. Oe, J. Appl. Phys. 54 (1983) 2052.

[28] C.P. Kuo, S.K. Vong, R.M. Cohen, G.B. Stringfellow, J. Appl. Phys. 57 (1985) 5428.

[29] S. Chen, X.G. Gong, S. Wei, Phys. Rev. B 75 (2007) 205209.

[30] N. Bouarissa, Phys. Stat. Solidi (b) 231 (2) (2002) 391–402.

[31] R.L. Anderson, Solid State Electron. 5 (5) (1962) 341–344.

[32] S. Chichibu, Y. Harada, M. Sugiyama, H. Nakanishi, J. Phys. Chem. Solids 64 (2003) 1481–1489.

[33] S. Kasap, P. Capper, Springer Handbook of electronic and Photonic Materials, Springer, New York, 2007.

[34] M.M. Islam, S. Ishizuka, A. Yamada, K. Sakurai, S. Niki, T. Sakurai, K. Akimoto, Sol. Energy Mater. Sol. Cells 93 (6-7) (2009) 970–972.

[35] K. Tanno, M. Ashokkumar, P. Mulvaney, D. Simpson, Colloids Surf. A: Physicochem. Eng. Aspects 141 (1) (1998) 143–151.

[36] S. Kobayashi, Y. Momiyama, F. Kaneko, Japan. J. Appl. Phys. 30 (10A) (1991) L1747.

[37] R. Lucena, J.C. Conesa, I. Aguilera, P. Palacios, P. Wahnón, V-substituted In_2S_3: an intermediate band material with photocalalytic activity in the whole visible light range, J. Mater. Chem. A 2 (2014) 8236–8245.